Finite element simulation of treatment with locking platefor distal fibula fractures

Yafeng Li (liyf@tiangong.edu.cn)
Tiangong University
Wei Yang
Tiangong University
Xi Zhang
Tianjin Hospital
Cheng Yu
Tiangong University
Zhengzhao Ji
Tiangong University
Jie Sun
Tianjin Hospital
Jing Zhang
Indiana University - Purdue University Indianapolis

Research Article

Keywords: distal fibula fracture, fibula model, finite element analysis, stress masking effect.

Posted Date: April 14th, 2022

DOI: https://doi.org/10.21203/rs.3.rs-1540013/v1

Abstract

In this study, an improved finite element model is applied to compare the biomechanical stability of plates with three different options in the treatment of distal fibula fractures. A CT scan of the knee to ankle segment of a volunteer was performed. A three-dimensional finite element model of the fibula was reconstructed based on the CT data. Three different loads (uni-pedal standing, torsion, and twisting) were applied, the same as in the experiments in the literature. The stresses and strains of the three options were compared under the same loads, using a 4-hole locking plate (Option A), a 5-hole locking plate (Option B), and a 6-hole locking plate (Option C) in a standard plate for lateral internal fixation. The simulation results show that all three options showed a stress masking effect. Option C had the best overall biomechanical performance and could effectively distribute the transferred weight. This is because option C has greater torsional stiffness and better biomechanical stability than options A and B, and therefore, option C is the recommended internal fixation method for distal fibula fractures. The finite element analysis method developed in this work is applicable to the stress analysis of fracture treatment options in other body parts.

1 Introduction

Distal fibular fractures account for approximately 3.92% of all fractures in the human body(Ju et al. 2019). Most distal fibula fractures require internal fixation, with plate internal fixation techniques being the most common. In the previous study (Fan et al. 2019), the use of a 4-hole angle stabilization plate and screws, in the clinical treatment of distal fibular fractures, improved the time of bone healing for eight weeks. In another study (Rozbruch et al. 1998), the 4-hole locking plate, 5-hole locking plate, and 6-hole locking plate internal fixation protocols were chosen. Another study (Fang et al. 2018) showed that the use of two to three screws would be sufficient for each major fracture block.

In parallel to experiments, the finite element model has been used to stimulate the bone healing process, with different screw layouts of the joint plate (Hess and Sommer 2011) (Cao et al. 2019). The relationship between the effective length of the plate on the stability of the tibiofibular was studied. Although the above efforts, there is still lacking how the stress and deformation occur in a realistic shaped distal fibula fracture.

In this study, an improved finite element model is proposed, which uses the reconstructed CT images. The developed model is firstly validated with experimental data in the literature. Then, in order to compare the biomechanical effectiveness and stability of different protocols in the treatment, three options with 4-hole, 5-hole, or 6-hole lateral internal fixation plates under different external loads (uni-axial compression, bending, and torsion) are considered. Their stress and displacement distributions are simulated. These results will be used to select the best treatment protocol for distal fibula fractures and provide theoretical understanding for clinical treatment.

2 Methods

2.1 CT scan data and geometry reconstruction

CT scan was conducted on the lower limb of a male volunteer patient (height 175 cm, weight 75 kg, age 29 years, and healthy lower limb bones). The 64-row spiral CT uses a scanning layer thickness of 0.5 mm. The CT data were converted to DICOM format and then imported into Mimics 20.0 software (Materialise, Belgium) to reconstruct the skin and cancellous bone into a 3D geometrical model in STL format. The fibula surface was processed by constructing grids and fitting surfaces in Geomagic Studio 13.0 software (Raindrop, USA), and then the solid model was created and exported into STEP format file.

2.2 Finite element modeling of internal fixation

The STEP format file was imported into Solidworks 20.0 (Dassault Systemes S.A, USA) for the assembly of the skin and cancellous bone. The models were imported into Anasys workbench 19.0 (ANSYS, USA) software for the finite element analysis.

Following the AO (Arbeitsgemeinschaft für Osteosynthesefragen) or the Association of the Study of Internal Fixation (ASIF) standard, the clavicle plate was assembled with the fibula fracture model according to the simulated surgery, thus completing the lateral internal fixation options of the distal fibula fracture.

The 4-hole lateral internal fixation plate model was defined as "Option A", the 5-hole lateral internal fixation plate model was defined as "Option B", and the 6-hole lateral internal fixation plate model was defined as "Option C ". The 4-hole, 5-hole, 6-hole locking plates, and screws were created. The threads of the screws were ignored in the model to simplify the computational time. As an example, the components and assembly of Option A are shown in Fig. 1a, which resemble the experimental setup in the literature (Knutsen et al. 2016). The screw and plate dimensions of the model are given in Table 1.

Table 1
Dimensions of three options of plates and screw

	Diameter (mm)	Length (mm)	Width (mm)	Height (mm)
(OptionA) 4-hole with bone plate	0	48	10	3
(Option B) 5-hole with bone plate	0	60	10	3
(Option C) 6-hole with bone plate	0	72	10	3
Screw	3.5	15	0	0

2.3 Material model

The cortical bone at the proximal and distal ends of the fibula is very thin, ~ 2 mm.

Therefore, the material properties of the outermost layer of the model were set to the cortical bone in the model. The material properties of the remaining parts were set to the cancellous bone, screw, and locking

plates, which are summarized in Table 2(Yang et al. 2021) (Shuangpeng et al. 2014).

Table 2
Material properties of the components in the finite element model (Yang et al. 2021) (Shuangpeng et al. 2014)

Material	Elastic modulus (MPa)	Poisson's ratio	Bone density (g/cm^3)	Yield strength (MPa)	Tensile strength (MPa)
Cortical bone	17,000	0.36	2.1	142	71
Cancellous bone	300	0.30	1.5	50	3.5
Locking plates	113,000	0.33	4.5	850	900
Screw	113,000	0.33	4.5	850	900

2.4 Mechanical load boundary conditions

In this study, three different mechanical boundary conditions are applied similar to the reference (Knutsen et al. 2016). Three types of loads were applied to the fibula model: (1) normal uni-pedal standing posture: a uniaxial compressive force of F = 200 N was applied to the fibular tuberosity with the full constraint of the external fibular ankle (Fig. 2 – 1). (2) Simulated bending motion: a moment of M = 1 N-m was applied at the fibular ankle, with the fibular head fully restrained (Fig. <link rid="fig2">2</link>–2). (3) Simulated torsional motion: a torsion moment of T = 1 N-m at the fibular tuberosity was used, and full constraint at the fibular external ankle (Fig. 2–3). The contact of steel plate, screw, skin, and cancellous bone were set as bound; the fracture surface was set as frictional contact with a friction coefficient of 0.2 (Galloway et al. 2013). It is noted that the fibula fracture has an exponential decrease in fibula model stiffness during prior simulation analyses (Cao et al. 2019), therefore, in this work no artificial cut was made at the outer ankle of the fibula to simulate a distal fibula fracture.

2.5 Validation test

To validate our model, the structural stiffnesses of options A, B, and C under torsional loading are calculated compared against the experimental test in the literature (Knutsen et al. 2016).

3 Results

3.1 Validation test results

The comparison of this model with the experimental result (Knutsen et al. 2016) is shown in Fig. 3. The comparisons suggest that the predictions are in reasonably good agreement with the experimental data. The structural stiffness of option A is 102% of that of the fibula assembled 5-hole pressurized plate, the

structural stiffness of option B is 116% of that of the fibula assembled 5-hole locking plate, and the structural stiffness of option C is 195% of that of the fibula assembled 6-hole tabbed plate.

3.2 Stress distributions

The peak stresses for three different options for various loads (Fig. 2) are analyzed. The summarized stress contours are given in Table 3.

Table 3: Simulated stress contours of fibula under different loads, with the maximum stress, labeled

Load type	Option A	Option B	Option C
Uni-axial load	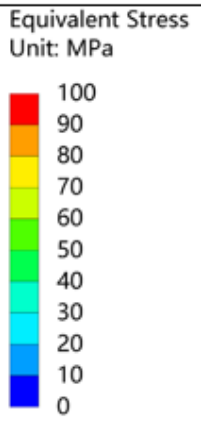 		
	96 MPa	98 MPa	91 MPa
Torsion load	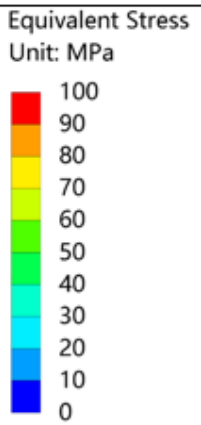 		
	99.9 MPa	97.3 MPa	71.4 MPa
Bend load	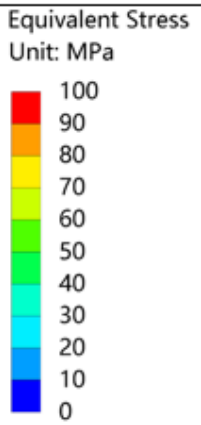 		
	49.5 MPa	56.2 MPa	50.0 MPa

In the fibula fracture model under uni-axial load, the maximum stresses for options A, B, and C all occurred at the plate nail connection at the fractured joint, with 96.6 MPa, 98.4 MPa, and 91.2 MPa, respectively. These peak stresses are much below the allowable failure strength. The maximum stresses on the fibula were 50.0 MPa, 51.7 MPa, and 54.1 MPa for the three options. Again all of them were less than the compressive strength of the cortical bone.

In the fibula fracture model under torque loading, the maximum displacements of options A and B occurred at the uppermost plate nail connection, which was 99.5 MPa and 97.3 MPa, respectively. In comparison, the maximum displacement of option C occurred at the plate connection at the bone joint, which was 71.4 MPa. The maximum stresses on the fibula were 17.3 MPa, 17.1 MPa, and 13.0 MPa, respectively. During the stress analysis, the stresses on the clavicle plate, screws, skin, and cancellous bone did not exceed the permissible strengths of their respective materials.

In the fibula fracture model under moment loading, the maximum displacements of options A, B, and C all occurred at the plate nail connection at the fractured joint, which was 49.5 MPa, 56.1 MPa, and 50.0 MPa, respectively. The maximum stresses on the fibula were 16.3 MPa, 15.3 MPa, and 14.6 MPa, respectively. Throughout the stress analysis, the stresses on the clavicle plate and screw did not exceed their strengths.

2.3 Comparison of the distribution of peak displacements for the three options

The displacement contours are summarized in Table 4. For the fibula fracture model under axial load, the maximum displacements of options A, B, and C all appeared at the fibular tuberosity, 8.79 mm, 8.40 mm, and 7.62 mm, respectively. Under the torque load, the maximum displacements of options A, B, and C appeared at the fibular tuberosity, which was 0.99 mm, 0.91 mm, and 0.88 mm, respectively. Under a bending moment load, the maximum displacements of options A, B, and C all occurred in the external ankle, which was 3.39 mm, 3.30 mm, and 3.10 mm, respectively.

Table 4: Displacement contours of the fibula under different loads, with maximum displacement values

Load type	Option A	Option B	Option C
Uni-axial load	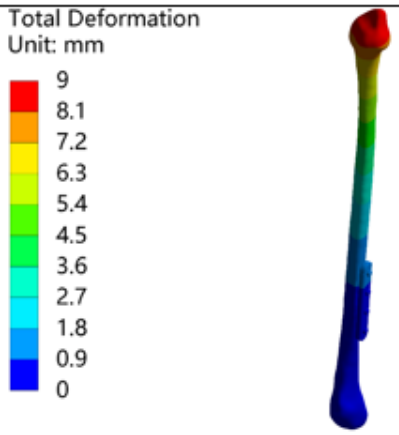	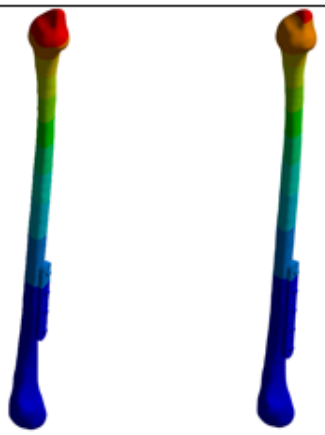	
	8.79 mm	8.40 mm	7.62 mm
Torsion load	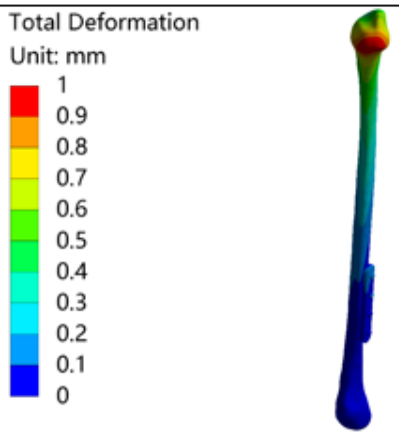	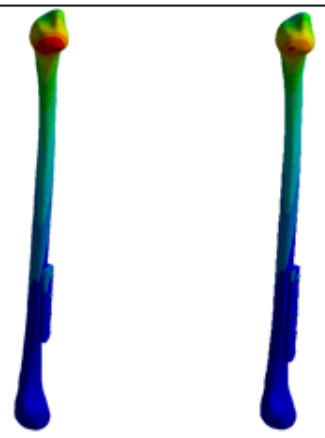	
	0.99 mm	0.91 mm	0.88 mm
Bend load	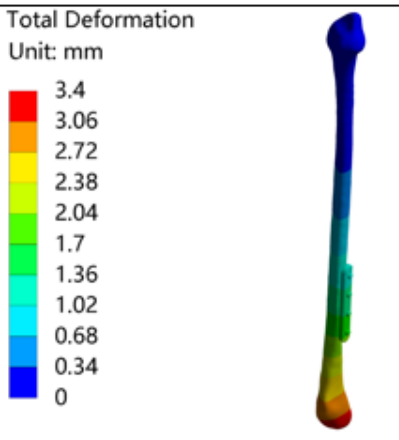		
	3.39 mm	3.30 mm	3.10 mm

4 Discussion

Peak stress and displacement values of fibula and plate under different options are summarized in Fig. 4. In this study, common fibula fractures and typical motions were analyzed using finite elements and other means. The results showed that the overall structural stiffness of Option C was the highest, and its resistance to bending and deformation was the strongest. In the surgical model of fibula fracture under axial load, the maximum stresses all appeared at the plate and nail connection near the fracture joint,

which is likely that the elastic modulus of the plate and screw is much larger than that of the fibula, and the stress masking phenomenon occurs near the fracture line.

For the approximate beam structure like the plate, the stresses are mainly concentrated near the fracture line under the action of gravity. Option C has smaller peak stresses and displacements compared with options A and B, indicating that the overall structural stiffness of the fibula is increasing with the increase in plate length and screws, and the use of relatively longer plates is beneficial to the recovery of the fibula, reducing the occurrence of delayed healing or nonhealing of the fibula after surgery and improving the structural stability of the distal fibular fracture. This is consistent with several clinical studies that have concluded that the use of relatively long plates is an important factor in reducing the risk of surgery (Ricci et al. 2014; Weber and Krause 2005).

In the surgical model of fibula fracture under torque loading, the peak stresses in the plates of options A and B appear in the uppermost screw. This may be caused by the stress concentration phenomenon between the plate and the fibula projection, which can be avoided by optimizing the shape of the plate. Therefore, movements such as flexion should be avoided during the early rehabilitation of fibular fractures, in order to avoid excessive stresses on the fibula and delay bone healing.

The maximum stresses on the fibula in options A, B, and C were all less than 20 MPa and the maximum displacements were all less than 3.40 mm in the surgical model of fibula fracture under bending moment loading, which was much less than the yield strengths of the plate and screw(Stoffel et al. 2003). Since the distal lateral fibula plate is on the extruded side, it is subjected to relatively small stresses and displacements. The results suggest that the choice of distal lateral fibula implantation plate is correct.

The stress contours of the fibula are shown in Fig. 5. It is noted that there is a stress masking phenomenon that occurs in all fractures under different loads (SL et al. 2012), which is due to a large difference between the elastic modulus of the titanium joint plate and that of the fibula. In this study, the stress masking phenomenon in option A at different loads is shown in Fig. 5. The stress values at the bone joints were lower than the stress stimulus required for normal bone growth, which is not helpful to bone healing.

5 Conclusions

In this study, an improved finite element modeling approach, based on reconstructed CT images, has been successfully developed. The model can simulate the physiological loading of the fibula after surgery, therefore exploring the best surgical solution for distal fibular fractures. The conclusions of the study according to the distal fibula fracture options are as follows:

1. The use of a relatively long plate (option C) will increase the overall structural stiffness of its surgical options, and improve its resistance to torsion and deformation.
2. With the use of metal plates, stress masking is inevitable at the fracture site. For non-load-bearing bones like the fibula, materials with elastic modulus close to that of the fibula should be considered.

This will reduce the stress masking effect, and the healing of the fibula can be facilitated.

Declarations

Ethics approval and consent to participate: The participant has the consent to participate in the study. The need for approval was waived.

Consent for publication: Not applicable.

Availability of data and materials: The datasets used and/or analyzed during the current study are available from the corresponding author on reasonable request.

Competing interests: The authors declare that they have no competing interests

Funding: Tianjin Education Scientific Research Project (2018KJ204) and China Scholarship Council (CSC) Scholarship.

Acknowledgments: Not applicable.

References

1. Cao Y, Zhang Y, Huang L, Huang X (2019) The impact of plate length, fibula integrity and plate placement on tibial shaft fixation stability: a finite element study J Journal of orthopaedic surgery research 14:1–7
2. Fan Z, Peng J, Zhou L, Hai-tao S, Huang Y, Wu J (2019) Meta-analysis of whether open reduction and internal fixation combined with thread anchors in the treatment of ankle fracture complicated with deltoid ligament injury J Chinese Tissue Engineering Study 23:1307–1312
3. Fang R, Ji A, Sheng W, Long D, Chen C (2018) Finite Element Analysis on Bone Healing Under Different Screw Configurations Journal of Medical Biomechanics 33:435–441
4. Galloway F, Kahnt M, Ramm H, Worsley P, Zachow S, Nair P, Taylor M (2013) A large scale finite element study of a cementless osseointegrated tibial tray J Journal of biomechanics 46:1900–1906
5. Hess F, Sommer C (2011) Minimally invasive plate osteosynthesis of the distal fibula with the locking compression plate: first experience of 20 cases J Journal of orthopaedic trauma 25:110–115
6. Ju DG, Debbi EM, Neustein AZ, Moon CN (2019) Fibular Lengthening Osteotomy With Revision Syndesmotic Repair for Ankle Fracture Malunion J Journal of orthopaedic trauma 33:S38-S39
7. Knutsen AR et al. (2016) Distal fibula fracture fixation: biomechanical evaluation of three different fixation implants J Foot Ankle Surgery 22:278–285
8. Ricci WM, Streubel PN, Morshed S, Collinge CA, Nork SE, Gardner MJ (2014) Risk factors for failure of locked plate fixation of distal femur fractures: an analysis of 335 cases J Journal of orthopaedic trauma 28:83–89

9. Rozbruch RS, Müller U, Gautier E, Ganz R (1998) The evolution of femoral shaft plating technique Clinical orthopaedics and related research 354:195–208
10. Shuangpeng D, wang C-t, JiBaoFen, Shu Z, JiaoYongZhe, lu4 Z, Chen C-s (2014) Parametric study on the influence of plant material selection and pretightening force on humerus J Chinese Journal of Bone and Joint Surgery 7:35–39
11. SL L, G T, DM W, SP D, CT W (2012) Finite element analysis in femoral fixation with medical 316L stainless steel plate Beijing Biomedical Engineering 31:445–449
12. Stoffel K, Dieter U, Stachowiak G, Gächter A, Kuster MS (2003) Biomechanical testing of the LCP–how can stability in locked internal fixators be controlled? Injury 34:B11-19
13. Weber M, Krause F (2005) Peroneal tendon lesions caused by antiglide plates used for fixation of lateral malleolar fractures: the effect of plate and screw position J Foot ankle international 26:281–285
14. Yang JC-S, Lin K-Y, Lin H-H, Lee OK (2021) Biomechanical evaluation of high tibial osteotomy plate with internal support block using finite element analysis J Plos one 16:e0247412

Figures

Figure 1

(a) Finite element assembly of the fibula fracture model (Option A) in this work, (b) experimental assembly (Knutsen et al. 2016).

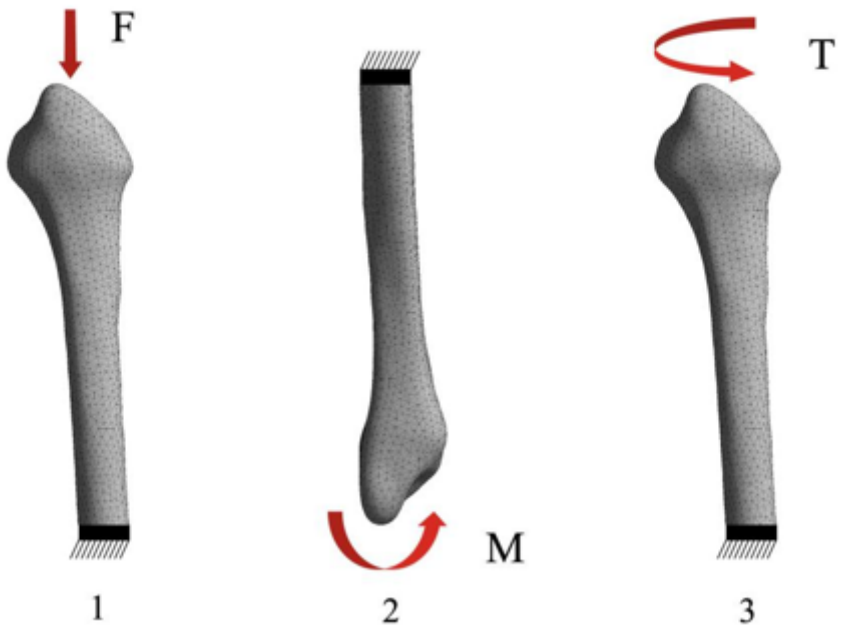

Figure 2

Schematic mechanical boundary conditions applied on the distal fibula fracture model (1) uni-axial compression force F, (2) bending moment M, and (3) torsion T.

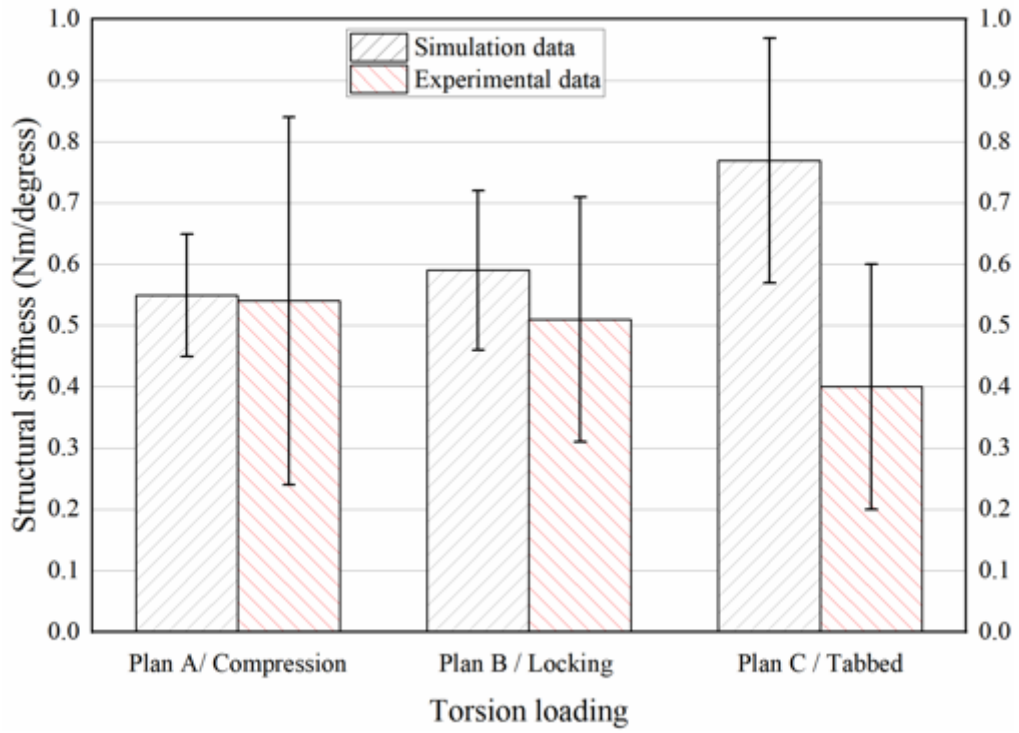

Figure 3

Structure stiffness comparison between the simulation in this study and experimental literature data (Knutsen et al. 2016)

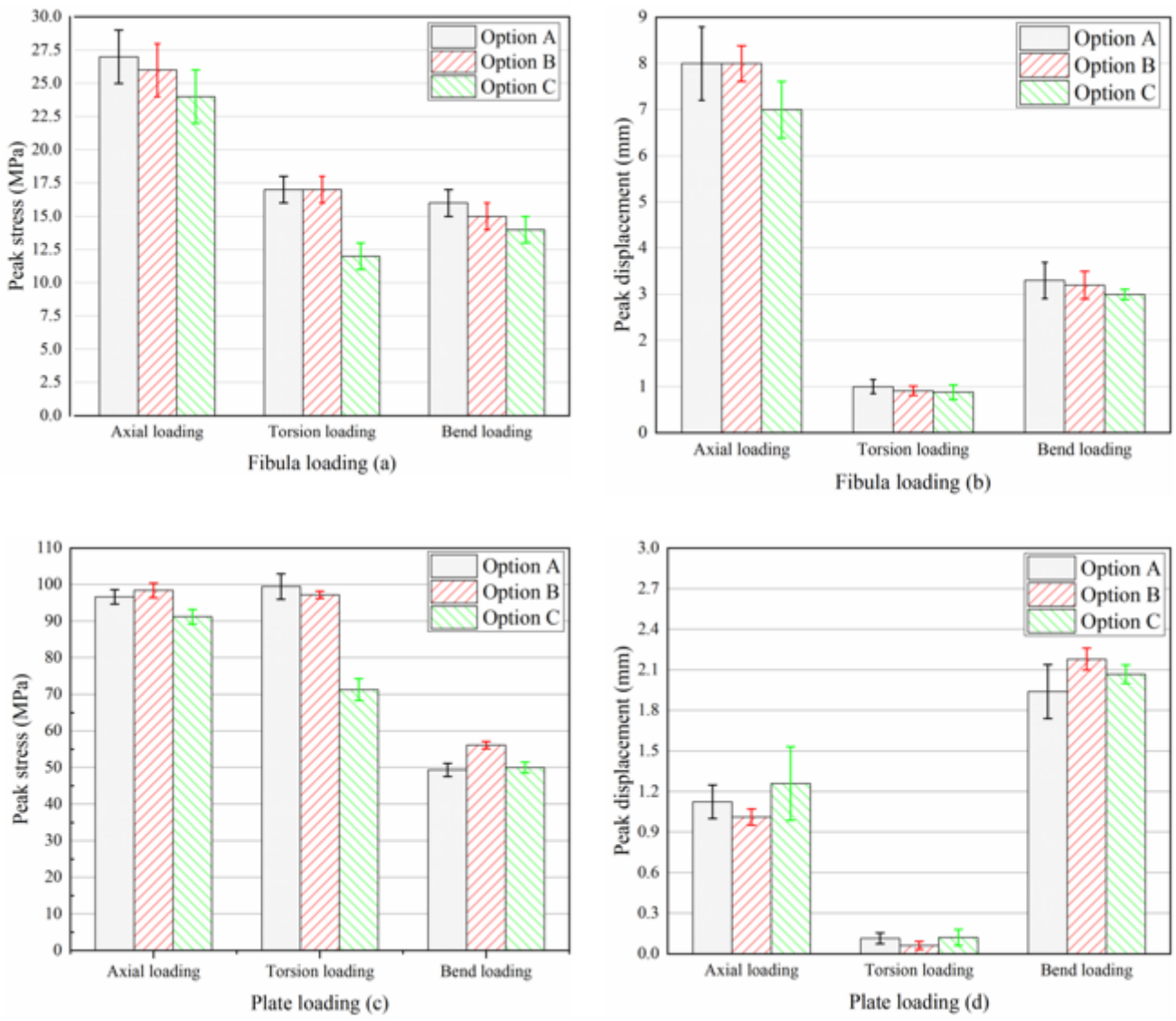

Figure 4

Peak stress and displacement values of fibula and plate under different options. (a) peak stress for fibula loading, (b) peak displacement for fibula loading, (c) peak stress for plate loading, and (d) peak displacement for plate loading

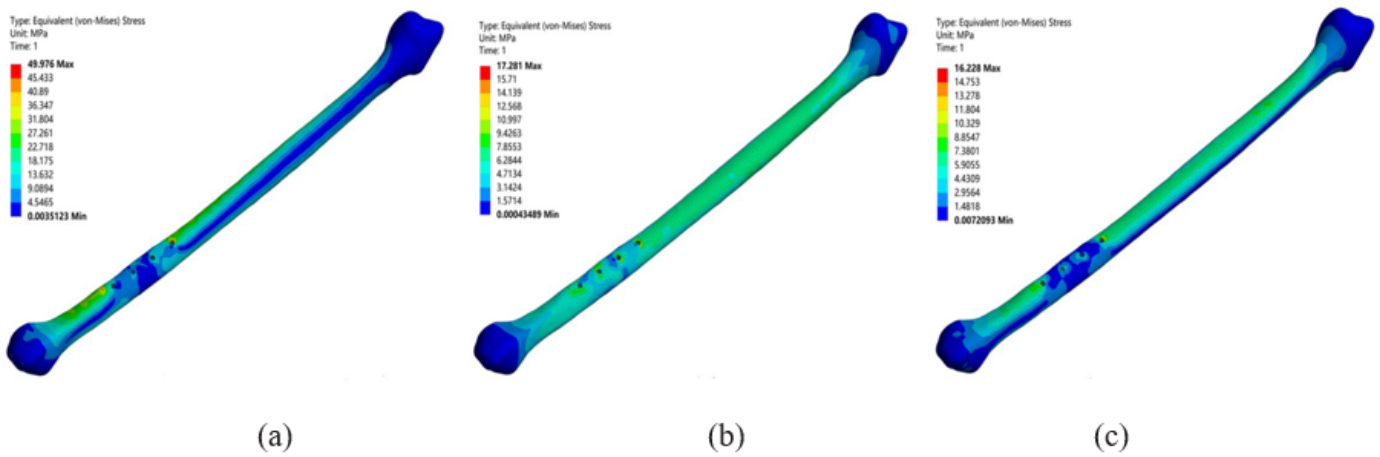

Figure 5

Stress contours of the fibula. (a) under uni-pedal stance, (b) torque loading, and (c) bending moment loading